bioRxiv preprint doi: https://doi.org/10.1101/123265; this version posted April 29, 2017. The copyright holder for this preprint (which was not certified by peer review) is the author/funder, who has granted bioRxiv a license to display the preprint in perpetuity. It is made available under aCC-BY 4.0 International license.

Pairwise hybrid incompatibilities dominate allopatric speciation for a simple biophysical model of development

Bhavin S. Khatri[*†,1] **and Richard A. Goldstein**[†]

[*]The Francis Crick Institute, London, United Kingdom, [†]Division of Infection & Immunity, University College London, London, United Kingdom

ABSTRACT

Understanding the origin of species is as Darwin called it "that mystery of mysteries". Yet, how the processes of evolution give rise to non-interbreeding species is still not well understood. In an empirical search for a genetic basis, transcription factor DNA binding has been identified as an important factor in the development of reproductive isolation. Computational and theoretical models based on the biophysics of transcription factor DNA binding have provided a mechanistic basis of such incompatibilities between allopatrically evolving populations. However, gene transcription by such binding events occurs embedded within gene regulatory networks, so the importance of pair-wise interactions compared to higher-order interactions in speciation remains an open question. Theoretical arguments suggest that higher-order incompatibilities should arise more easily. Here, we show using simulations based on a simple biophysical genotype phenotype map of spatial patterning in development, that biophysics provides a stronger constraint, leading to pair-wise incompatibilities arising more quickly and being more numerous than higher-order incompatibilities. Further, we find for small, drift dominated, populations that the growth of incompatibilities is largely determined by sequence entropy constraints alone; small populations give rise to incompatibilities more rapidly as the common ancestor is more likely to be slightly maladapted. This is also seen in models based solely on transcription factor DNA binding, showing that such simple models have considerable explanative power. We suggest the balance between sequence entropy and fitness may play a universal role in the growth of incompatibilities in complex gene regulatory systems.

KEYWORDS speciation, Dobzhansky-Muller incompatibilities, sequence entropy, population size, co-evolution, genotype phenotype map

Introduction

The detailed genetic mechanisms by which non-interbreeding species arise is still largely not understood. Darwin called it that "mystery of mysteries" (Darwin 1859); he struggled to understand how natural selection could give rise to hybrid inviability or infertility. In a modern setting, Darwin's conundrum can be stated as follows: if a hybrid incompatibility were due to a single locus, how could two species, fixed for AA and aa, respectively, evolve from a common ancestor, if the only evolutionary pathway is via the inviable genotype Aa? A solution to this problem was conceived independently by Dobzhansky (1936), Muller (1942), Bateson (1909), by which neither population need pass through a bottleneck. If instead incompatibilities arise due to non-linear or epistatic fitness interactions between different loci, it is possible, for example, that two lines that are geographically isolated from each other, evolve independently from a common ancestor ab (allopatric evolution), fix the allelic combinations aB and Ab respectively, yet the hybrid genotype AB is inviable.

The work of Orr provided a framework to understand how incompatibilities might arise in allopatry (Orr 1995; Orr and Turelli 2001), when populations are small and essentially monomorphic ($\mu N \ll 1$, where μ is the mutation rate for a typical loci and N the effective population size). Orr suggested that as two lines fix

Copyright © 2017 by the Genetics Society of America
doi: 10.1534/genetics.XXX.XXXXXX
Manuscript compiled: Saturday 29th April, 2017%
[1]Division of Infection & Immunity, University College London & The Francis Crick Institute, London, United Kingdom, bhavin.khatri@physics.org

bioRxiv preprint doi: https://doi.org/10.1101/123265; this version posted April 29, 2017. The copyright holder for this preprint (which was not certified by peer review) is the author/funder, who has granted bioRxiv a license to display the preprint in perpetuity. It is made available under aCC-BY 4.0 International license.

independent substitutions from a common ancestor, any combination of alleles that may arise in hybrids that have not been 'tested' or explicitly fixed by the process of evolution, represents a potential incompatibility. Assuming an infinite number of loci and that back-substitutions or multiple substitutions at the same loci are not possible, Orr showed that the number of incompatibilities involving n-loci increases as $\sim K^n$, for K substitutions separating the two lines and assuming $n \ll K$. This has been likened to a "snowball" effect as the number of incompatibilities rises rapidly with the number of substitutions that separate the lines. Orr also argued that more complex DMIs, which involve more than 2 loci, should be easier to evolve as there is a larger fraction viable evolutionary paths between the common ancestor genotype and the genotypes of the two present day species, for a fixed number of incompatible genotypes (Orr 1995). It is, however, an open question, as this argument predicates, whether the number of incompatible genotypes remains fixed as the number of loci increases, for more realistic fitness landscapes.

To address the question of how incompatibilities develop in more realistic fitness landscapes, Tulchinsky et al, developed sequence-based simulations that investigated the mechanistic basis of the evolution of hybrid incompatibilities for transcription factor-DNA binding, showing decreased hybrid fitness for smaller populations (Tulchinsky *et al.* 2014b) and that the pleiotropic constraint of binding two sites does not significantly affect how quickly incompatibilities arise (Tulchinsky *et al.* 2014a). Khatri and Goldstein (2015a,b) used a similar model, based on a simple biophysically motivated genotype-phenotype map of a single transcription factor binding to DNA; they notably found that incompatibilities arose more quickly for smaller, drift-dominated, populations as they are already more slightly maladapted. This arises as there are exponentially more sequences that bind poorly than well, which means drift pushes common ancestors on average closer to incompatible regions and so fewer substitutions are needed for incompatibilities to arise in hybrids. In this low population size limit DMIs arise quadratically with divergence time, in agreement with Orr's predictions, however, the underlying mechanism for this power law is very different to Orr's. Conversely, larger population sizes are on average more optimal with respect to binding and so more substitutions are required in order for hybrids to become incompatible. In addition, these substitutions themselves arise more slowly as the number of neutral substitutions decrease with increasing population size, in accordance with predictions of the nearly neutral theory (Ohta 1973, 1992; Lanfear *et al.* 2014). In this case the growth of DMIs has a characteristic non-power law form, with negative curvature on a log-log plot, indicating that the hybrid binding energies change diffusively (Khatri and Goldstein 2015a,b). However, real gene regulatory systems are more complex than a single TF binding to DNA, so again the question arises do these predictions hold for more complex gene regulatory systems with more realistic fitness landscapes?

Although there has been much progress in understanding evolution in terms of selection, mutation and genetic drift, the majority of this work has been reliant on phenomenological fitness landscapes, which encompass in a heuristic manner smoothness, epistasis and neutrality (Higgs and Derrida 1992; Kauffman and Levin 1987). In recent years, the question of the structure of real fitness landscapes has gained prominence, where the redundancy of the mapping from genotype to phenotype can give rise to non-trivial properties of the evolution of phenotypes (Fontana 2002; Khatri *et al.* 2009; Hayden *et al.* 2011; Goldstein 2011; Schaper and Louis 2014; Greenbury *et al.* 2014; Manrubia and Cuesta 2015; Greenbury *et al.* 2016). In particular, (Khatri *et al.* 2009) introduced a simple genotype-phenotype map for spatial gene expression regulation in development, from which emerged a number of non-trivial features such as a balance between selection and sequence entropy deciding the course of evolution at small population sizes and a partitioning of the effective phenotypic landscape into neutral and selective degrees of freedom; none of these emergent phenomena could be predicted on the basis of purely phenotypic considerations.

In this paper, we will use a slightly modified version of the spatial patterning model in Khatri *et al.* (2009), which has explicit sequence representation of each loci, to examine the growth of Dobzhansky-Muller incompatibilities in allopatry as a function of population size and under stabilising selection in each lineage. Our results show that smaller populations develop incompatibilities more quickly and in a manner mostly predicted based solely on simple models of transcription factor DNA binding, showing the power of these simple approaches (Khatri and Goldstein 2015a,b; Tulchinsky *et al.* 2014b,a); the main difference we find is that for large populations hybrid binding energies are sub-diffusive, indicative of kinetic traps in the molecular substitution process due to an underlying roughness to the fitness landscape (Khatri *et al.* 2009). However, our main finding is that unlike Orr's prediction, pair-wise interactions between loci dominate the growth of DMIs, suggesting that biophysics provides a stronger constraint on their evolution than the simple combinatorics of pathways between the common ancestor and present day lineages.

Materials and Methods

Genotype-Phenotype map

The genotype-phenotype map we use is a slight modification of the one described in detail by Khatri *et al.* (2009); we summarise its basic elements and recapitulate the main results in the Supporting Information. The evolutionary task set for the gene regulation module is to turn an exponentially decaying morphogen gradient across a field of cells in an embryo (M), into a sharp step function profile of a downstream transcription factor TF with its transition at the mid-point of the embryo, as shown in Fig.1. The binding affinity of the different protein species to themselves or to the regulatory region of TF is determined by matching binary sequences, generating the genotype-phenotype map; there are two types of binding energies, protein-DNA binding energies denoted by E and protein-protein denoted by δE. More specifically, gene regulation is controlled by two non-overlapping binding sites, the promoter P and an adjacent binding site B, together with two protein species, the morphogen M and RNA Polymerase R, where the length of each of these sequences, $\boldsymbol{r}_{pd}, \boldsymbol{m}_{pd}, \boldsymbol{t}_P, \boldsymbol{t}_B$ is $\ell_{pd} = 10$. Co-operative protein-protein interactions between the morphogen M and RNA Polymerase R, or themselves, are determined by the sequences, $\boldsymbol{r}_{pp}, \boldsymbol{m}_{pp}$, each of length $\ell_{pp} = 5$. The various binding energies are proportional to the Hamming distance between the relevant sequences, where for protein-DNA binding the cost of a mismatch is $\epsilon_{pd} = 2k_BT$ and for protein-protein interactions $\epsilon_{pp} = 1k_BT$. In total this gives a genome $\boldsymbol{G} = [\boldsymbol{r}_{pd}, \boldsymbol{r}_{pp}, \boldsymbol{m}_{pd}, \boldsymbol{m}_{pp}, \boldsymbol{t}_P, \boldsymbol{t}_B]$, of total length $|\boldsymbol{G}| = 50$, producing 4 protein-DNA binding energy traits ($E_{RP}, E_{RB}, E_{MP}, E_{MB}$) and 3 protein-protein binding energy traits ($\delta E_{RR}, \delta E_{RM}, \delta E_{MM}$).

Given an exponential morphogen concentration profile

bioRxiv preprint doi: https://doi.org/10.1101/123265; this version posted April 29, 2017. The copyright holder for this preprint (which was not certified by peer review) is the author/funder, who has granted bioRxiv a license to display the preprint in perpetuity. It is made available under aCC-BY 4.0 International license.

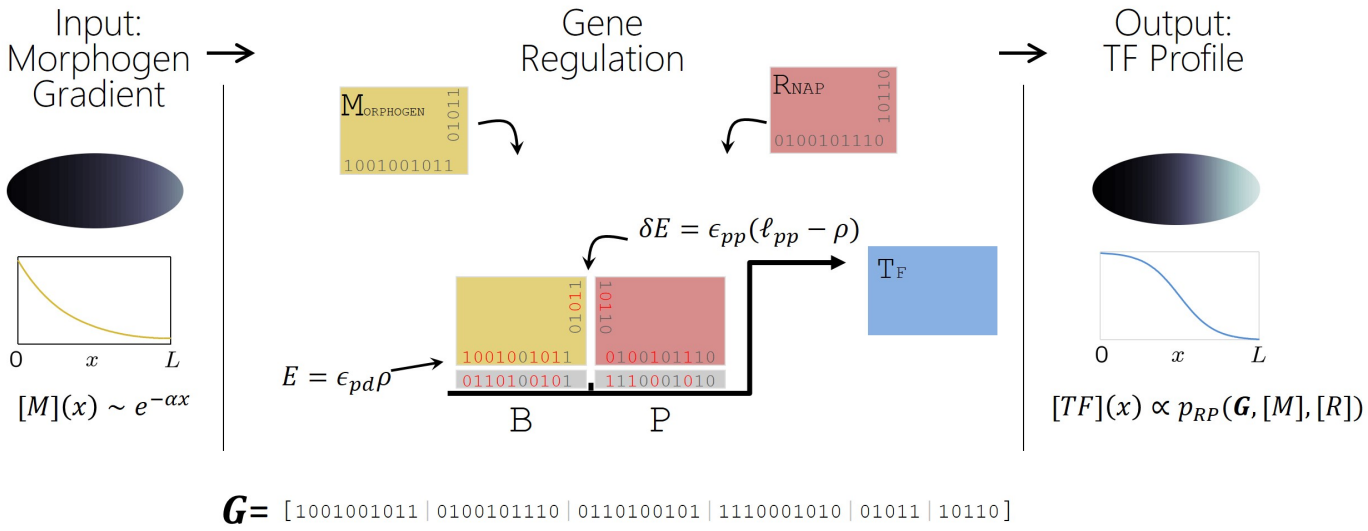

Figure 1 An overview of the genotype-phenotype map. The gene regulatory module has input a morphogen gradient $[M](x)$ across a 1-dimensional embryo of length L and outputs a transcription factor $TF(x)$. Gene regulation of TF using a morphogen and RNAP (R) is controlled in a bottom-up manner, by binding to its regulatory region consisting of a promoter P and adjacent binding site B; E represents binding free energies of proteins to one of the two binding sites of the regulatory region of the transcription factor T, δE are protein-protein free energies to aid in co-operative binding of paired protein complexes. Each energy is calculated by the number of mismatches ρ (Hamming distance), shown in red, between relevant binary sequences, together with mismatch energies ϵ_{pd} and ϵ_{pp} for protein-DNA and protein-protein energies respectively. Transcription of T is controlled by the probability of RNAP being bound to the P, p_{RP}.

$[M](x, \alpha)$ as a function of the position of embryonic cells, x, and a fixed concentration $[R]$ of RNAP, in each cell, we follow Shea and Ackers (1985) to calculate the TF concentration profile $[TF](x)$, which assumes the steady state concentration profile is simply proportional to the probability of RNAP being bound to the promoter: $[TF](x) \propto p_{RP}(\boldsymbol{G}, R, M(x, \alpha))$. The proportionality constant is given by the ratio of the rate of transcription and translation to the rate of degradation of TF, which is not important in our study, since we are only interested in the shape or contrast of $[TF](x)$ that can be achieved.

Monte Carlo Scheme for speciation simulations

We use a kinetic Monte Carlo scheme to simulate a Wright-Fisher evolutionary process for the genome $\boldsymbol{G}$ and α on two independent lineages, as detailed in Khatri and Goldstein (2015b). The rate of fixation of one-step mutants are calculated based on Kimura's probability of fixation (Kimura 1962), where we assume a regime of small effective population size ($|\boldsymbol{G}|\mu_0 N \ll 1$, where μ_0 is the base-pair mutation rate and N is effective population size). Here, we determine the Malthusian or log fitness of the spatial gene regulation, from the resulting concentration profile $[TF](x)$ by use of a functional that promotes expression of the TF in the anterior half, whilst penalising expression in the posterior half, with truncation selection below a critical value W^*:

$$F = \begin{cases} \kappa_F \ln(\mathcal{W}) & \text{if } \mathcal{W} > W^* \\ -\infty & \text{if } \mathcal{W} < W^* \end{cases} \qquad (1)$$

where,

$$\mathcal{W}[[TF](x)] = \frac{\int_0^{L/2}[TF](x)\mathrm{d}x - \int_{L/2}^{L}[TF](x)\mathrm{d}x}{\frac{L}{2}\max_x\{[TF](x)\}}. \qquad (2)$$

where W^* is related to the threshold for inviability and κ_F is the strength of selection for the trait represented by the spatial patterning process; when the hybrid's log-fitness drops below $F^* = \kappa_F \log(W^*)$ an incompatibility or DMI arises. We choose $W^* = 0.2$ to give a reasonable number of incompatibilities that arise in a simulation, where typically the maximum of $\mathcal{W} \approx 0.6$. Note that although here the exact form of the fitness is slightly different to the one used in Khatri *et al.* (2009), the qualitative behaviour is the same (Supporting Information).

The speciation simulations consist of two replicate simulations starting with the same common ancestor and with the same fitness function. We draw the common ancestor from the equilibrium distribution for $\boldsymbol{G}$ and α. To do this we start from a random initial genome, and run one long simulation for 100,000 substitutions for a fixed scaled population size $2\kappa_F N$, in order to effectively equilibrate the system (typically 10,000 substitutions are required to adapt to an ensemble of fit states). This represents a reference equilibrium state; different random draws from the equilibrium distribution then consist of running the simulation for a further 100 substitutions.

Decomposing DMIs

Our genome is composed of 4 loci: 1) RNAP, (whose sequence is $\boldsymbol{g}_R = [\boldsymbol{r}_{pd}, \boldsymbol{r}_{pp}]$), 2) Morphogen (sequence, $\boldsymbol{g}_M = [\boldsymbol{m}_{pd}, \boldsymbol{m}_{pp}]$), 3) Regulatory region of TF ($\boldsymbol{g}_T = [\boldsymbol{t}_P, \boldsymbol{t}_B]$) and 4) the morphogen gradient steepness α. Hybrids between the two lines are constructed by independent reassortment of these loci and assuming

bioRxiv preprint doi: https://doi.org/10.1101/123265; this version posted April 29, 2017. The copyright holder for this preprint (which was not certified by peer review) is the author/funder, who has granted bioRxiv a license to display the preprint in perpetuity. It is made available under aCC-BY 4.0 International license.

complete linkage within each loci. We define a hybrid genotype by a 4 digit string where each digit corresponds to one of the loci defined above and takes one of two values, which correspond to the allele from the 1st line or 2nd line; for example, the hybrid rMTa corresponds to R locus having an allele from the 1st lineage, M locus with the allele from the 2nd lineage, T locus from the 2nd lineage and α locus the allele from the 1st lineage. Note that the underlying sequence of each hybrid changes as different substitutions are accepted in each lineage; the notation only refers to alleles fixed at any point in time. As α is a continuous variable, we only count substitutions in α when it makes a transition between the two basins of attraction as discussed in Khatri *et al.* (2009) and the Supporting Information.

We can represent all combinations of the four loci drawn from the two parents (RMTA, RMTa, RMtA, etc.) as points on a four-dimensional Boolean hypercube (Fig.2). If there is a 2-point DMI (e.g. between T and α loci, which we denote I_{Ta}), then all four hybrid-genotypes containing this DMI (e.g. RMTa, RmTa, rMTa, rmTa) are inviable; these genotypes define a two-dimensional subspace (or face) of the hypercube. Similarly, the points (e.g. rmtA, RmtA, which we denote I_{mtA}) containing a 3-point DMI form a one-dimensional subspace (or line), while a 4-point DMI takes up only a single point in the four-dimensional hypercube. These different 2-point, 3-point and 4-point DMIs are the fundamental incompatibility types which we seek to explain the pattern of hybrid inviable genotypes observed, for example, as in Fig.2a.

However, this decomposition is hugely underdetermined, as there are only $2^4 - 2 = 14$ possible hybrids (not including the well-adapted genotypes of line 1 and line 2) and a total of $I_{max} = 3^L + 1 - 2^{L+1} = 50$, different fundamental incompatibilities, for $L = 4$ loci [1]. The approach we take is to find only those combinations of fundamental DMIs that have the smallest total number that can explain the pattern of hybrid incompatibilities, which from a Bayesian perspective would have the smallest Occam factors (MacKay 2007); for instance, as shown in Fig.2a the list of 6 incompatible hybrid genotypes rmTa, rMTa,RmTa,RMTa,Rmta,RMta, shown by red crosses, can be explained most parsimoniously by three different minimal combinations of fundamental DMIs, each with only 2 DMIs: 1) $I_{\mathsf{Ta}} + I_{\mathsf{Rta}}$, 2) $I_{\mathsf{Ra}} + I_{\mathsf{rTa}}$, 3) $I_{\mathsf{Ta}} + I_{\mathsf{Ra}}$. We assume each of these minimal combinations of DMIs is a priori equally likely, so we count the number of type I_{Ta} DMIs as the average times they appear across this set of minimal combinations of DMIs; in the example in Fig.2a, the number of each type of fundamental DMI would be $n_{Ta} = 2/3$, $n_{Ra} = 2/3$, $n_{Rta} = 1/3$, $n_{rTa} = 1/3$, so the total number of 2-point DMIs is $n_2 = 4/3$ and 3-point DMIs $n_3 = 2/3$, giving a total number of $n = n_2 + n_3 = 2$ DMIs, which is the minimum number of DMIs needed to explain the pattern of hybrid incompatibilities. In Fig.2b is shown a more complicated pattern of hybrid DMIs and the parsimonious minimal combinations of fundamental DMIs.

[1] The total number of $n-$point DMIs is $(2^n - 2)\binom{L}{n}$, as there are $\binom{L}{n}$ combinations of n loci amongst L total loci and then considering a binary choice of alleles across both lines, there are a total of 2^n allelic combinations or states, 2 of which are the fit allelic combinations where all alleles come from one lineage or the other giving $2^n - 2$. For example, between each pair of loci there are $2^2 - 2 = 2$ mismatching combinations of alleles (e.g. rM and Rm) that could give DMIs and $\binom{L}{2} = L(L-1)/2 = 6$ pairwise interactions. A similar argument would give a total of 24 3-point DMIs as there are $2^3 - 2 = 6$ mismatching combinations of alleles at 3 loci (e.g., excluding rmt and RMT) and $\binom{L}{3} = 4$ 3-point interactions and similarly, $14\binom{L}{4} = 14$ for 4-point interactions. In total, the max number of DMIs is $I_{max} = \sum_{n=2}^{L}(2^n - 2)\binom{L}{n} = 3^L + 1 - 2^{L+1}$, which for $L = 4$ loci is $I_{max} = 50$.

Results

Evolutionary properties of genotype-phenotype map on each lineage

The properties of this genotype-phenotype map have been previously explored (Khatri *et al.* 2009). An important property of this genotype-phenotype map is that only a single mechanism of patterning is found, which is that RNAP (R) binds with intermediate affinity to the promoter (P), but through a high affinity protein-protein interaction with the morphogen (M), the morphogen binds to the first binding site (B) only above a critical morphogen concentration, thereby giving a spatial switch once the morphogen falls below this concentration; evolution then fine tunes the relationship between the protein-DNA binding energies (E's), protein-protein energies (δE's) and the steepness of the morphogen gradient α to turn off transcription at the mid-point of the embryo. Despite a single global solution there are many different combinations of the binding and glue energies and α that give good patterning, and for each of these many underlying genotypes ($\boldsymbol{G}$). A further key property is that despite this redundancy some energy phenotypes such as $E_{MB}, \delta E_{RM}$ and E_{RP} are under strong stabilising selection, whilst the remaining energy phenotypes, $E_{RB}, E_{MP}, \delta E_{RR}$ and δE_{MM} are under weak stabilising selection (see Supporting Information and Khatri *et al.* (2009)). Finally, at large population sizes it is found that the evolutionary dynamics exhibits what is known as quenched-disorder in statistical physics, where energy phenotypes that are less constrained take different *random* values between independent evolutionary runs; this indicates an underlying roughness to the fitness landscape (Khatri *et al.* 2009).

Different hybrids genotypes have different growth rates of DMIs

In Fig.3, we plot a typical time series of how the fitness of two different hybrids (Rmta a & b and RMtA c & d) changes over a divergence time t separating a pair of lines, for scaled population sizes of $2N\kappa_F = 1$ and $2N\kappa_F = 10$. A scaled population size $2N\kappa_F > 1$ indicates strong selection, whilst $2N\kappa_F \leq 1$ indicates weak selection, where genetic drift dominates over selection; for example, in human populations it has been estimated that $\approx 20\%$ of mutations are weakly selected (Eyre-Walker *et al.* 2006). We see that the fitness of hybrids generally decreases in a stochastic fashion; when the fitness of a hybrid drops below the threshold F^* (indicated by the dashed line), a DMI arises and is indicated by a vertical fitness line ($F = -\infty$) for that hybrid and so as we see from Fig.3, at any given time only a subset of all possible hybrids might be incompatible. We also see that as the fitness of hybrids is stochastic, DMIs that arise do not stay, as one might expect within the Orr framework (Orr 1995; Orr and Turelli 2001). A further observation is that for smaller scaled population sizes the common ancestor fitness is lower and incompatibilities appear to arise more quickly; this is a consistent with previous studies of a more simple genotype-phenotype map of a transcription factor binding a single binding site (Khatri and Goldstein 2015a,b), where the smaller populations have a larger genetic drift load and so common ancestors are more likely to be closer to the inviable binding threshold.

To examine the overall trends in the number of incompatibilities for each hybrid type, as a function of divergence time μt, we plot the average number of DMIs in Fig.4, where we have averaged over pairs of complementary genotypes (e.g. RmtA and rMTa), which have identical statistical properties. As denoted in

bioRxiv preprint doi: https://doi.org/10.1101/123265; this version posted April 29, 2017. The copyright holder for this preprint (which was not certified by peer review) is the author/funder, who has granted bioRxiv a license to display the preprint in perpetuity. It is made available under aCC-BY 4.0 International license.

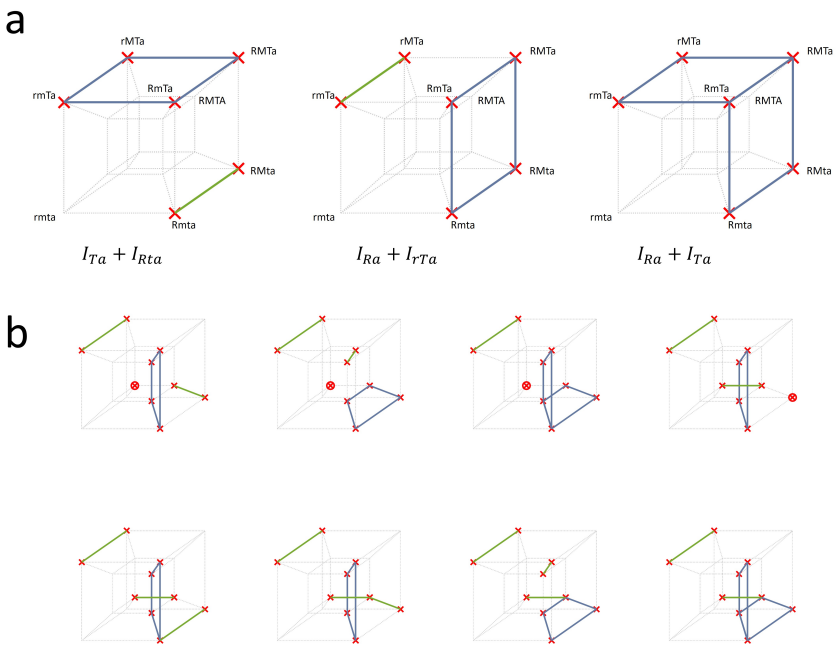

Figure 2 Decomposition of hybrid DMIs on a Boolean hyper 4-cube. Each point on the 4-cube represent each possible hybrid genotype across 4 loci, including the genotype of each parental lineage, where each red cross represents an incompatible hybrid genotype. As shown in a) the pattern of DMIs can be explained by different combinations of fundamental types of DMIs, where a blue square or face identify a subspace of genotypes that correspond to a 2-point DMI and a single green edge or line corresponds to a 3-point DMI. b) A more complicated pattern of hybrid DMIs and their decomposition into fundamental types, where a red open circle corresponds to a single isolated 4-point DMI.

the figure, we distinguish hybrid-genotypes based on the types of potential mismatch: R-type is characterised by a mismatch of the R loci with M and T loci, M-type is a mismatch of M with R and T loci, T-type is a mismatch of T with R and M and α-type is a mismatch of the α loci with the rest of the loci. In Fig.4, we first note that each hybrid-genotype behaves in a different way in a population size dependent manner. In general, there is an initial growth in the average number of DMIs as the divergence time increases, followed by a plateau or a slowing down of the growth. We also see that for small population sizes the initial growth of DMIs is power law and approximately quadratic, as predicted by Orr (1995); Orr and Turelli (2001), but as argued previously (Khatri and Goldstein 2015b) the underlying mechanism is very different. On the other hand, as the population size increases, DMIs take longer to arise, which is also consistent with previous work on the dynamics of incompatibilities due to transcription factor DNA binding (Khatri and Goldstein 2015b); this is caused by a slowing of the substitution rate as in a stabilising discrete fitness landscape more deleterious changes are needed for any evolutionary change. Further, there is no clear power law, which is again consistent with previous simulations (Khatri and Goldstein 2015b) and also theoretical calculations (Khatri and Goldstein 2015a) that predict that as common ancestor populations are further away, the growth of DMIs follows a diffusive law, which has a characteristic negative curvature on a log-log plot.

However, in addition to these general trends, we see that the growth of DMIs is different for different hybrids; for small population sizes ($2N\kappa_F = 0.1$ & $2N\kappa_F = 1$), M-type, T-type and R-type dominate the growth of DMIs, in this order and with only a small difference between them, whilst α-type arise far more slowly; we might expect this since substitutions in α only tend to shift the pattern away from the mid-point of the embryo, which with the model of fitness defined in Eqn.1 only moderately affects fitness. As the population size increases, and at small times, we see that initially M-type DMIs arise more slowly relative to T-types and R-types, but at longer times there is a cross-over where M-type DMIs dominate R-type; although the simulations do not run out to sufficiently long times for the largest population sizes, this cross-over appears to move to longer times at increasing population sizes.

How can we understand this general behaviour? It is clear from Eqns. 1&2 that good patterning or fitness is only dependent on the protein-DNA and protein-protein energy phenotypes (as well as α) and so this in general requires co-evolution of the relevant sequences to maintain these energies within certain constraints; e.g. the binding energy of R to the promoter of T, E_{RP} mustn't be too strong and so on each line the sequences will co-evolve to maintain this constraint. From previous work (Khatri and Goldstein 2015a,b) we expect that it is not only the population size that determines how quickly hybrid incompatibilities arise, but its product with the strength of selection κ_j maintaining a particular interaction j; so the energy E_{MB} is under very strong selection for strong binding of the morphogen to the 1st binding site and we would expect incompatibilities due to this interaction to arise more slowly when $2N\kappa_{MB} \gg 1$, due to $\kappa_{MB} > \kappa_j$, for other interactions j, even when the effective population size N is fixed.

bioRxiv preprint doi: https://doi.org/10.1101/123265; this version posted April 29, 2017. The copyright holder for this preprint (which was not certified by peer review) is the author/funder, who has granted bioRxiv a license to display the preprint in perpetuity. It is made available under aCC-BY 4.0 International license.

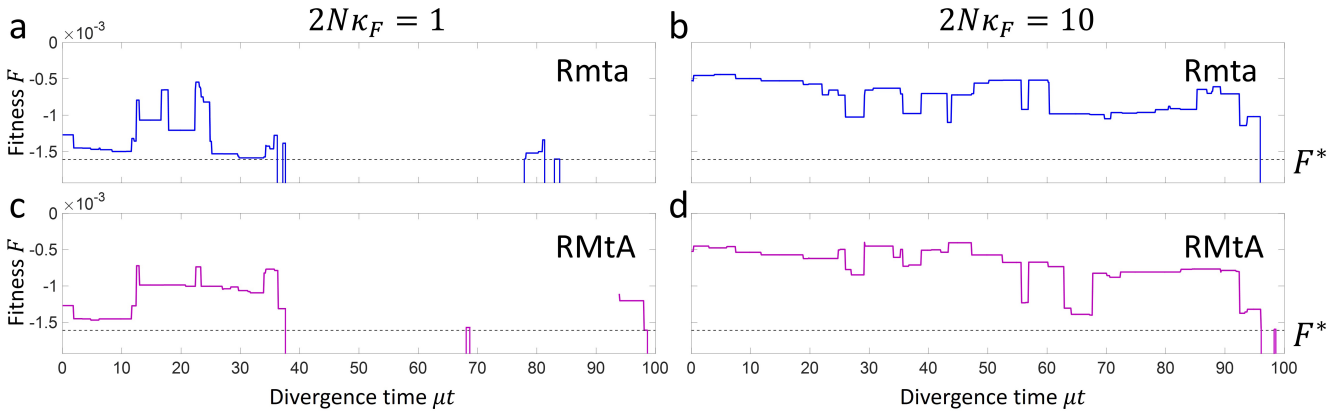

Figure 3 Plot of the times series of two hybrids Rmta (a & b) and $RMtA$ (c & d) at scaled population sizes of $2N\kappa_F = 1$ (a & c) and $2N\kappa_F = 10$ (b & d).

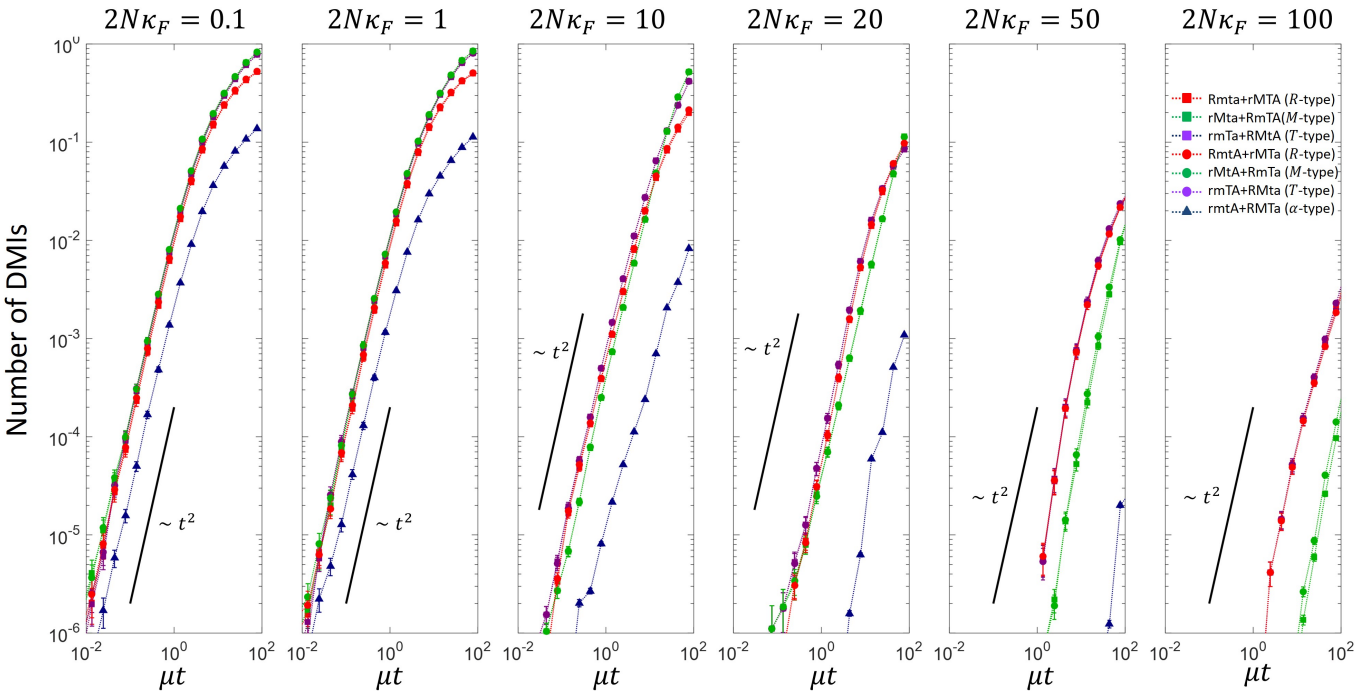

Figure 4 Plot of the number of DMIs for each hybrid genotype since divergence for different scaled population sizes. Complementary hybrid genotypes are summed over, since they have identical statistical properties.

bioRxiv preprint doi: https://doi.org/10.1101/123265; this version posted April 29, 2017. The copyright holder for this preprint (which was not certified by peer review) is the author/funder, who has granted bioRxiv a license to display the preprint in perpetuity. It is made available under aCC-BY 4.0 International license.

Decomposition of DMIs

As discussed in the model section the DMIs shown in Fig.4 will have contributions from many different fundamental incompatibility types, which can be 2-point, 3-point and 4-point in nature. Using the method described above to decompose DMIs into fundamental types, we plot the total number of each type of DMI versus divergence time in Fig.5, where the panels correspond to different scaled effective population sizes from $2N\kappa_F = 0.1$ to $2N\kappa_F = 100$. We see clearly that pair-wise DMIs are dominant at all population sizes and divergence times, though the difference is diminished at larger population sizes. These results show that contrary to the prediction of Orr, that higher order DMIs should be easier to evolve, higher order DMIs evolve more slowly and are in smaller number compared to pair-wise DMIs.

As mentioned in the introduction the Orr model also predicts that n-point DMIs should increase as $\sim t^n$. Here, we find that for small population sizes 2-point, 3-point and 4-point DMIs all increase as a power law at small times, indicated by a straight line on a log-log plot, with a larger exponent for 3-point and 4-point DMIs. To more quantitatively assess the exponent, we fit the data for $2N\kappa_F \leq 20$ using the phenomenological equation:

$$I(t) = \frac{I_0 t}{T+t}\left(1 - \exp\left(-t/\tau\right)^{\gamma-1}\right) \tag{3}$$

which has the asymptotic form of $I(t) \sim t^\gamma$ for $t \ll \tau$ and $t \ll T$ and an opposite limit of $I(t \to \infty) = I_0$. We see that for the total number of DMIs and for 2-point, 3-point and 4-point DMIs, this form fits the data well at intermediate and small population sizes. We tabulate the power law exponent derived from these fits in Table 1. We see that the total number of DMIs and 2-point DMIs have a power law exponent close to $\gamma = 2$, which is consistent with the Orr model and with Fig.4 which shows a similar power law, further showing that 2-point DMIs are dominant in determining the growth of hybrid incompatibilities. However, the higher order incompatibilities do not quite follow the Orr prediction, where n-point DMIs should have an exponent $\gamma = n$, although 4-point DMIs have a larger exponent than 3-point DMIs; 3-point DMIs have an exponent that varies between $\gamma = 2$ and $\gamma = 3$, while 4-point DMIs have an exponent between $\gamma = 3$ to $\gamma = 3.5$. In all these cases an alternative model for the power law behaviour, as argued in Khatri and Goldstein (2015b), is that at small population sizes, where genetic drift is dominant and there is a large drift load, common ancestor populations are poised at the incompatibility boundary (truncation selection threshold) and the growth of DMIs at short times is due to how likely a few critical substitutions are to arrive very quickly, which is given by a Poisson process; if the critical number of substitutions is K^* then for short times we would expect $P_I(t) \sim (\mu t)^{K^*}$ and so given that at least n substitutions are needed for a n-point incompatibility, we would expect $K^* \geq n$. It is possible the inconsistency here could be resolved by more accurate measurement of the power law, by exploring simulations at even shorter times, using a larger number of replicate simulations (here there are 10^6 replicate simulations at short times).

At larger population sizes ($2N\kappa_F \geq 50$), Fig.5 shows that there is no clear power law and instead there is a negative curvature in the growth of DMIs on a log-log plot. This is consistent with a model of DMI growth where high fitness corresponds to high binding affinity, so that the common ancestor distribution is peaked away from the inviability boundary; this would arise with large populations that have a small drift load, meaning that

$2N\kappa_F$	0.1	1	10	20
Total	1.94 ± 0.05	1.99 ± 0.05	1.95 ± 0.05	2.00 ± 0.12
2-point	1.93 ± 0.05	1.98 ± 0.06	1.84 ± 0.06	1.97 ± 0.13
3-point	2.66 ± 0.13	2.81 ± 0.17	2.76 ± 0.24	2.14 ± 0.15
4-point	3.17 ± 0.19	3.43 ± 0.41	3.14 ± 0.24	2.93 ± 0.19

Table 1 Table of values of the exponent γ characterising the power law of growth of DMIs at short times and small scaled population sizes.

DMIs arise as hybrid energy traits diffuse to the boundary. One such analytically tractable model was investigated in Khatri and Goldstein (2015a) and predicted that the number of DMIs is a complementary error function, which has an asymptotic form $I(t) \sim \frac{\sqrt{4\mu t}}{K^*} e^{-(K^*)^2/4\mu t}$, which due to the essential singularity as $t \to 0$ has the property of negative curvature on a log-log plot. However, this form does not fit the simulation data well (not shown). Given the multidimensional nature of this spatial patterning model, it is possible that we need to consider the analogous result to the effective one-dimensional diffusion studied in Khatri and Goldstein (2015a), which results in a multidimensional generalisation of the error function Brown (1963), where in n dimensions $\mathrm{erf}_n(x) = \Gamma(x^2, n/2)/\Gamma(n/2)$, so that the number of DMIs has asymptotic form $I(t) \sim (\frac{4\mu t}{K^*})^{1-\frac{n}{2}} e^{-(K^*)^2/4\mu t}$; this again, however, does not fit the data in Fig.5 well. A functional form that is a good fit to the data at large populations sizes is

$$I(t) = \frac{\sqrt{4(\mu t)^\beta}}{K^*} e^{-(K^*)^2/4(\mu t)^\beta}, \tag{4}$$

which arises when considering fractional Brownian processes with exponent β; normal diffusion or Brownian motion arises when $\beta = 1$, while $\beta < 1$ corresponds to *sub*diffusive behaviour, while $\beta > 1$ is *super*diffusive. It is clear by examining the exponent β in Table 2 from fits of the data in Fig.5 at large population size ($2N\kappa_F \geq 50$) that the DMIs arise as a result of a subdiffusive process, where 2-point, 3-point and 4-point DMIs have an exponent $\beta \approx 1/3$ for $2N\kappa_F = 50$ and $\beta \approx 1/4$ for $2N\kappa_F = 100$. The most likely mechanism that would give rise to subdiffusive behaviour is a broad spectrum of times between substitutions; even though in the simulations the kinetic Monte carlo scheme is based on a Poisson process for a given genotypic state $\boldsymbol{G}$, the distribution of rates could vary significantly as populations explore the fitness landscape. This would be consistent with the results in Khatri *et al.* (2009), which reveal the underlying fitness landscape of this spatial patterning genotype-phenotype map to be rough, which could lead to broad distribution of substitution rates in each lineage and effective subdiffusive behaviour of the hybrids (Bertin and Bouchaud 2003). Finally as expected the average number of substitutions needed at large population sizes is large, with values of K^* ranging from 6 to 9, and increases with increasing population size, as expected; it also increases very moderately with increasing n, which would be consistent an increase in dimensionality of higher order DMIs. Interestingly, these values of K^* would indicate that the fraction of viable genotypes is very small, $\sim 2^{K^*}/2^{|\boldsymbol{G}|} \sim 10^{-13}$, where $|\boldsymbol{G}| = 50$ is the number of binary sites in this genotype-phenotype map.

bioRxiv preprint doi: https://doi.org/10.1101/123265; this version posted April 29, 2017. The copyright holder for this preprint (which was not certified by peer review) is the author/funder, who has granted bioRxiv a license to display the preprint in perpetuity. It is made available under aCC-BY 4.0 International license.

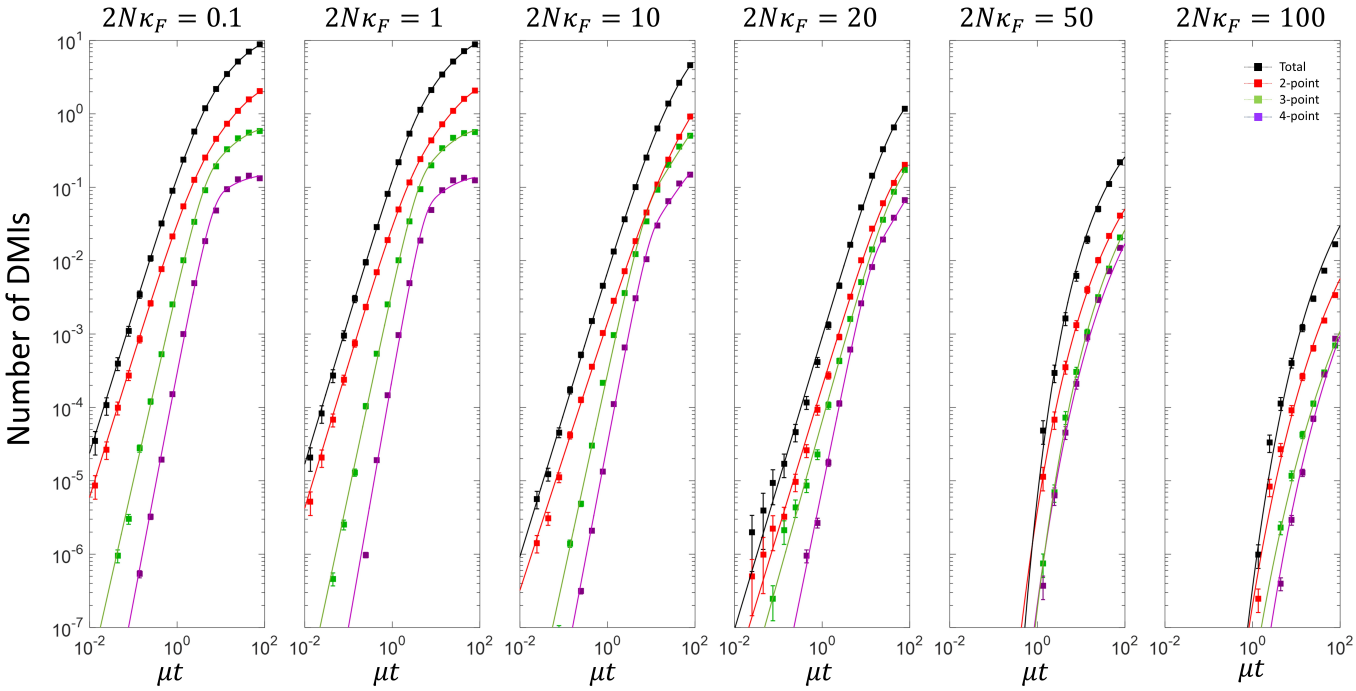

Figure 5 Plot of the total number of DMIs vs divergence time, together with their decomposition into the total number of 2-point, 3-point, 4-point DMIs, for various scaled populations sizes. For $2N\kappa_F \leq 20$ the solid lines correspond to fits of the simulation data to Eqn.3, while for $2N\kappa_F \geq 50$ correspond to fits to Eqn.4.

$2N\kappa_F$		50	100
Total	β	0.47 ± 0.03	0.33 ± 0.02
	K^*	6.58 ± 0.12	7.37 ± 0.26
2-point	β	0.32 ± 0.01	0.25 ± 0.01
	K^*	6.71 ± 0.07	7.51 ± 0.18
3-point	β	0.33 ± 0.01	0.22 ± 0.01
	K^*	7.53 ± 0.10	8.09 ± 0.27
4-point	β	0.31 ± 0.02	0.25 ± 0.02
	K^*	7.50 ± 0.28	8.66 ± 0.39

Table 2 Table of values of the parameters characterising the sub-diffusive growth of DMIs for large scaled population sizes; $\beta = 1$ corresponds to normal diffusive motion, $\beta < 1$ to sub-diffusion and $\beta > 1$ super-diffusion, while K^* corresponds roughly to the number of substitutions required to reach the invaible region.

2-point DMIs In Fig.6 we have plotted the number of 2-point DMIs of each type, where for example, I_{mt} is a 2-point DMI caused by an incompatibility between the M locus and T locus. First, we note that at small population sizes the rate of increase of the different 2-point incompatibilities seem to cluster into two types; those that involve α and those that do not, which arise more rapidly; this suggests that sequence entropy constraints are dominating for small populations, particularly at short times, though for the latter group there are some differences as discussed below. As the population size increases, we see that differences arise in the rate of growth between these different types of 2-point incompatibilities. Below we discuss below these properties.

For each type of 2-point incompatibility there are 2 binding energy traits that could contribute. So increases in I_{mt} could be due to an incompatibility in the hybrid of E_{MB} or E_{MP}; in this case, as the binding energy E_{MP} is almost neutral (Khatri *et al.* 2009), we would would expect incompatibilities to arise predominantly from E_{MB}. Similarly, we expect I_{rt} to be dominated by E_{RP} and not E_{RB} and I_{rm} dominated by δE_{RM} and not δE_{MM} or δE_{RR}. When it comes to incompatibilities involving the α-locus, there is no clear phenotypic trait that can be identified and as we will see the analysis of these DMIs will not be so clear.

Examining Fig.6, we see at small population sizes, $2N\kappa_F \leq 1$, that all the DMIs grow approximately quadratically at short times with a saturating form at long times, as also seen in Fig.5. In addition, we see that when population sizes are small, the number of DMIs for a particular pair-wise interaction correlates with the strength of selection on that trait, though the differences are relatively small as noted above; for example, the binding energy trait E_{MB}, which has the strongest selective constraint, gives rise to the most number of DMIs (I_{mt}) at all times; the next most critical energy trait in terms of selective constraint is δE_{RM},

bioRxiv preprint doi: https://doi.org/10.1101/123265; this version posted April 29, 2017. The copyright holder for this preprint (which was not certified by peer review) is the author/funder, who has granted bioRxiv a license to display the preprint in perpetuity. It is made available under aCC-BY 4.0 International license.

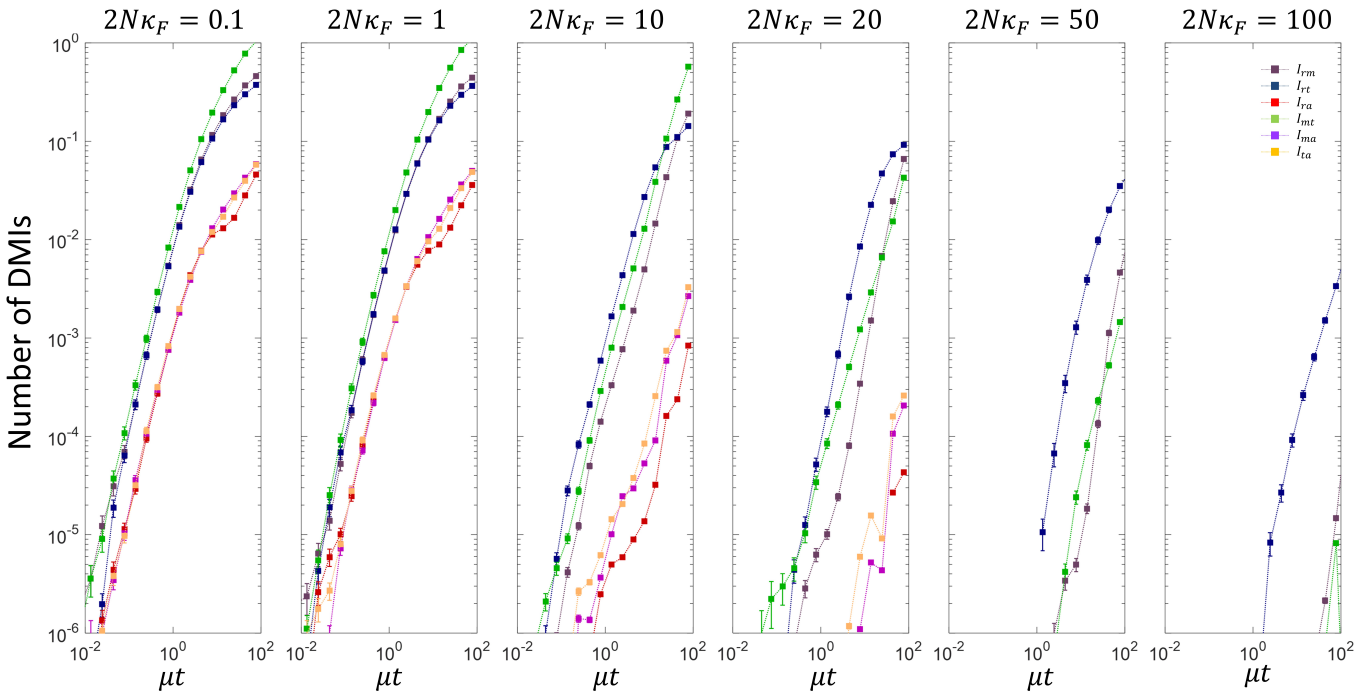

Figure 6 Plot of the spectrum 2-point DMIs vs divergence time for different scaled population sizes.

which has the next highest number of DMIs (I_{rm}). Although, this observation would appear to be intuitive, interpreting it in light the results of a simple model of transcription factor DNA binding (Khatri and Goldstein 2015b) are not straightforward; the results of this work suggest that for small population sizes, the rate that incompatibilities arise decreases with increasing strength of selection, since their common ancestors are on average better adapted. However, the same model also predicts that the rate of growth of incompatibilities decreases with sequence length, as phenotypes coded by longer sequences evolve more quickly, so it is possible these two effects could confound each other. Here for example, E_{MB} has a stronger selective constraint compared to δE_{RM}, but a longer sequence length, as each DNA-protein interaction interface has 10 binary digits versus each protein-protein interaction interface that has 5. Also it is not clear how a single inviability threshold F^* effectively maps to these pair-wise incompatibilities, complicating the picture further.

However, as the scaled population size increases, we see that the time for I_{mt} incompatibilities to arise sharply increases, while the time for I_{rm} increases less rapidly and I_{rt} even less rapidly. This is consistent with the simple model of transcription factor DNA binding described in Khatri and Goldstein (2015b) and as observed with the hybrid DMIs in Fig.4, as E_{MB}, which contributes most to I_{mt} is under the greatest selection pressure and so as the population size changes these should change most rapidly. We see that for large population sizes, it is not the phenotypic traits under the strongest selection that give rise to significant DMIs at short times, but those under a weaker selective constraint; traits under weaker selection will be affected more by the sequence entropic pressure for poorer binding affinities and so the common ancestor is more likely to be closer to the inviability boundary. However, if a trait is effectively neutral, i.e. that selection is sufficiently weak that for no trait values can incompatibilities arise, then these will not give rise to incompatibilities; the energy traits E_{RB}, E_{MP}, δE_{RR} and δE_{MM} have this property, as is evident by examining their marginal distribution functions which follow the neutral expectation (Khatri *et al.* 2009).

The 2-point incompatibilities involving the α locus are more difficult to interpret, since there is no clear trait in the patterning model associated with an interaction solely between the α locus and R, M, or T loci; if α was resolved into a sequence for a protease and its interaction with a 3rd sequence of the M loci, in addition to the sequences for protein-DNA and protein-protein binding, then the value of α itself would be a trait determined by a pair-wise interaction between this 3rd sequence of M and the protease loci, but the current model does not include this feature. The most identifiable phenotype associated with α is the position of the mid-point of the embryo, but this trait involves a co-evolution of E_{MB} and α and so represents a 3-point interaction between M, T and α loci, which will be discussed below. It is likely that the 2-point DMIs involving α are spurious and a consequence of the parsimonious DMI decomposition method used, which assumes an equal prior on all possible DMIs that have a minimum number of DMI types. This could be rectified by having a zero-prior on all pair-wise incompatibilities involving the α locus; however, here we have not implemented this as 2-point DMIs involving α are typically an order of magnitude smaller than the other DMIs.

3-point & 4-point DMIs In Fig.7, we have plotted the 3-point DMIs as a function of divergence time μt, where the panels from left to right represent increasing scaled population size. We see that for small population sizes, 3-point DMIs between the R, M and T loci dominate at all times and in particular that the different types of DMIs of this type are all roughly equal, $I_{Rmt} \approx I_{rMt} \approx I_{rmT}$. In addition, we see that all other DMIs arise more slowly and each of the 9 other types of 3-point DMIs are all again approximately equal. However, at larger population sizes

bioRxiv preprint doi: https://doi.org/10.1101/123265; this version posted April 29, 2017. The copyright holder for this preprint (which was not certified by peer review) is the author/funder, who has granted bioRxiv a license to display the preprint in perpetuity. It is made available under aCC-BY 4.0 International license.

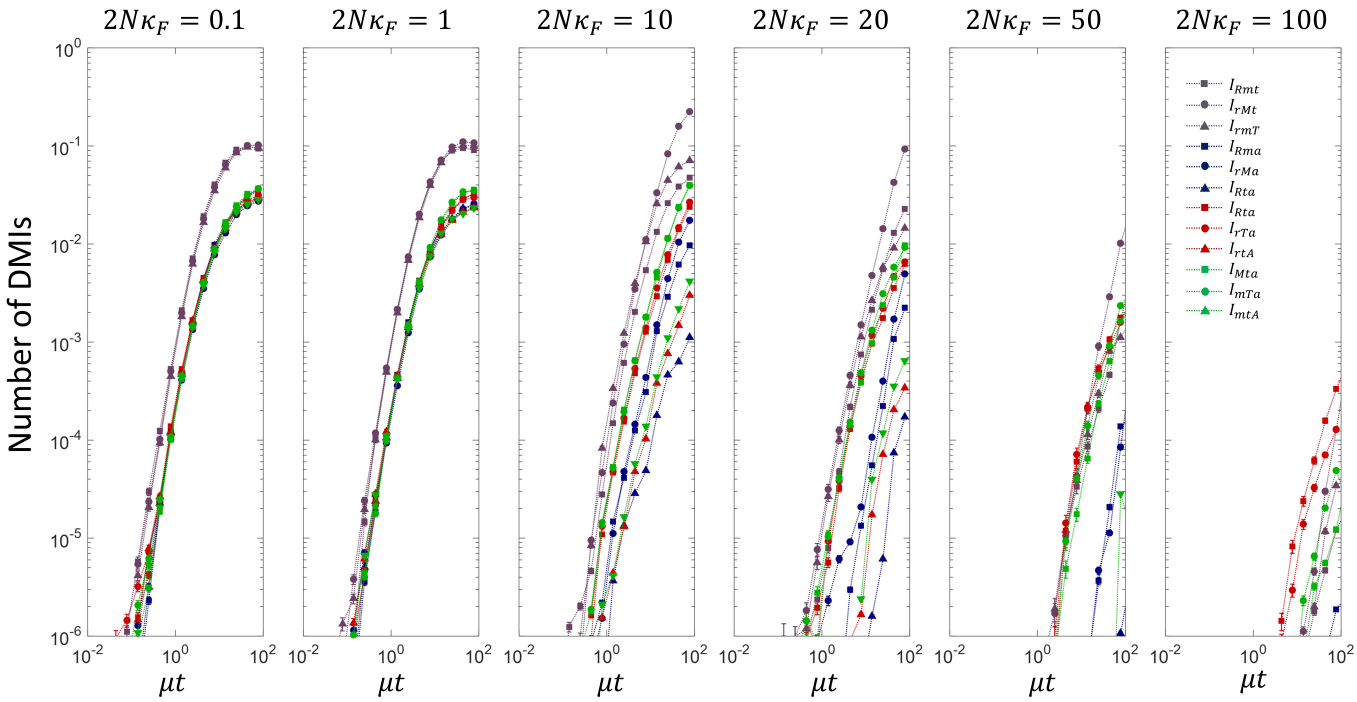

Figure 7 Plot of the spectrum 3-point DMIs vs divergence time for different scaled population sizes.

this degeneracy is lifted amongst the different types of DMIs and different 3-point DMIs grow at different rates. How can we understand this general behaviour?

The patterning solution found in these evolutionary simulations involves the morphogen binding strongly to the first binding site recruiting RNAP to bind to the promotor to turn on transcription, through a high affinity interaction between the morphogen and RNAP; the spatial position along the length of the embryo where the transcription switches from on to off is controlled by an interaction with the steepness of the morphogen gradient α. Given this, incompatibilities between R, M and T loci could arise through a 3-point interaction where the R loci interacts with the parts of the T and M loci coding for E_{RP} and δE_{RM}, or where M loci interacts with the parts of the T and R loci coding for E_{MB} and δE_{RM}. So in analogy to 2-point DMIs, where a pair of loci give rise a single phenotypic binding energy trait, whose value contributes to fitness, here the triplet of loci, R, M and T, give rise to two binding energy traits, which together contribute to fitness. These two traits will co-evolve to maintain good fitness, balanced by the constraints of sequence entropy on the underlying 3 loci; at large population sizes, the effects of sequence entropy will diminish. On the other hand 3-point incompatibilities between, for example, M, T and α could arise due to an interaction of the E_{MB} binding energy trait with α; in this model this is subject to a sequence entropy constraint between only two loci. This is true for all the 3-point interactions that involve the α loci. Qualitatively, this then explains the behaviour at low population sizes, as sequence entropy dominates fitness, meaning that the behaviour of the different 3-point DMIs will be dominated by their underlying sequence entropy constraints.

The sequence entropy constraints for the 3-point interactions involving the α loci is straightforward and given by a binomial degeneracy function $\Omega(E) = \binom{\ell}{E/\epsilon}$, so that the sequence entropy function $S(E) = \ln(\Omega)$ is approximately quadratic in E, where here E represents one of the binding energies that interacts with α. However, for the other 3-point interactions that don't involve α, but involve the R, M and T loci, the sequence entropy constraint will be related to a degeneracy function $\Omega(E, \delta E) = \Omega(E)\Omega(\delta E)$, where the joint number of sequences that give E and δE is a product, since these energy traits are coded by different sequences, even though they come from the same loci (the joint number of sequences $\Omega(E_{MB}, E_{MP}) \neq \Omega(E_{MB})\Omega(E_{MP})$ since the protein binding sequence of the morphogen that determines E_{MB} and E_{MP} is the same in this case). Given that the joint number of sequences that give E and δE is a product of two binomial coefficients, the sequence entropy function will approximately be a sum of two quadratic terms $S(E, \delta E) \approx -\frac{2}{\ell_{pd}}(E/\epsilon_{pd} - \ell_{pd}/2)^2 - \frac{2}{\ell_{pp}}(\delta E/\epsilon_{pp} - \ell_{pp}/2)^2$. At small population sizes, where genetic drift dominates selection, we expect the distribution of common ancestors to be such that they are poised at the incompatibility boundary for E and δE; incompatibilities then arise when substitutions arise that take hybrids across the boundary.

Given that a 3-point DMI between the R, M and T genetic loci corresponds to co-evolution of a pair of binding energy traits, instead of a single binding energy trait for 2-point and 3-point DMIs that involve α, means the fraction of substitutions that lead to incompatibilities versus those that keep the hybrids compatible/fit becomes larger when going from one to two dimensions. This then explains why 3-point DMIs between the R, M and T loci gives rise to incompatibilities more quickly than those involving the α loci, as seen in Fig.7. Also since at small population sizes the only influence that fitness will have is in defining the region of incompatibility for the traits of interest, we see that for each type of DMI there are very little differences in the rate of growth of DMIs.

4-point DMIs correspond to an interaction where all four loci require a particular combination of alleles for good patterning. As previously noted they are of much smaller number compared

bioRxiv preprint doi: https://doi.org/10.1101/123265; this version posted April 29, 2017. The copyright holder for this preprint (which was not certified by peer review) is the author/funder, who has granted bioRxiv a license to display the preprint in perpetuity. It is made available under aCC-BY 4.0 International license.

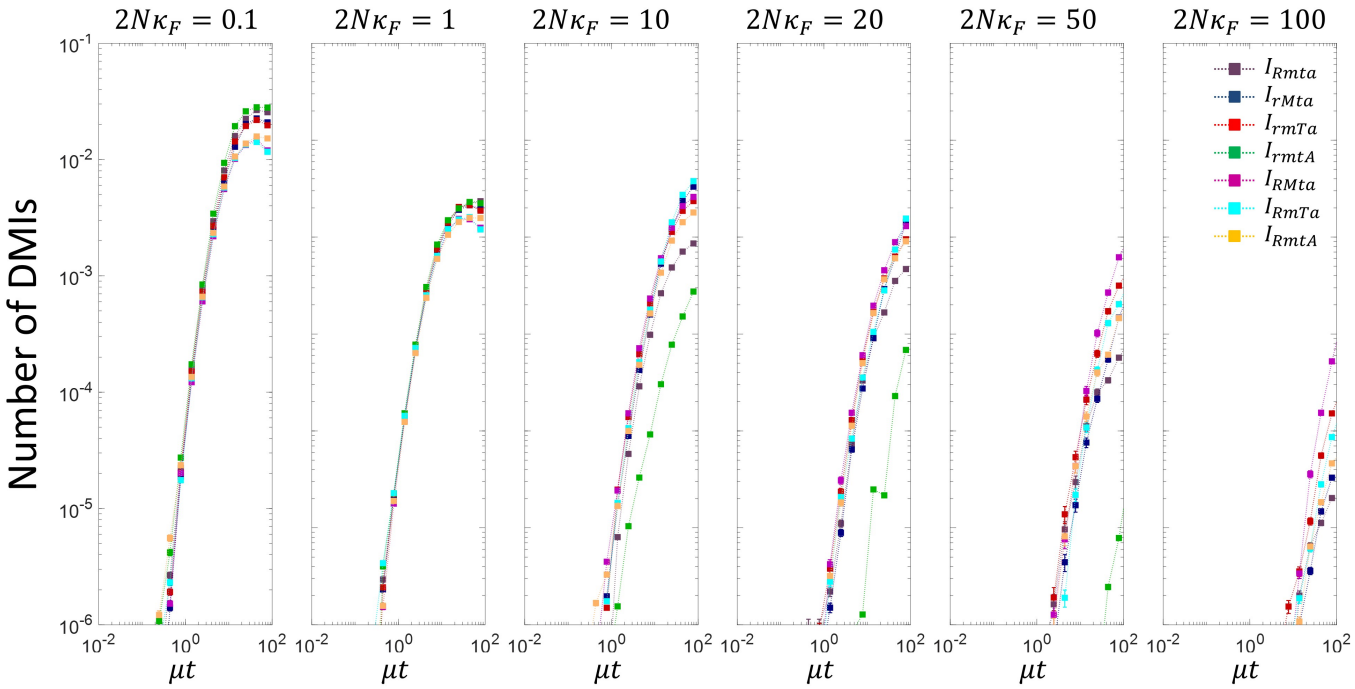

Figure 8 Plot of the spectrum 4-point DMIs vs divergence time for different scaled population sizes.

to 2- and 3-point DMIs, so here, we do not examine these DMIs in detail. However, we note that the 4-point DMIs shown in Fig.8, show a similar pattern as found with 3-point DMIs, where for small scaled population sizes the DMIs tend to cluster, which suggests, as found for 2- and 3-point DMIs, this is due to sequence entropy constraints dominating the growth of DMIs; on the other hand, at large scaled population sizes this degeneracy is lifted and each hybrid has a different growth rate of DMIs, depending on their particular contribution to fitness and how that balances against the constraints of sequence entropy.

Discussion

There is still very little understood about the underlying genetic basis that gives rise to reproductive isolation between lineages. Gene expression divergence is thought to be a strong determinant of the differences between species (King and Wilson 1975; Wolf *et al.* 2010; Wray 2007; Abzhanov *et al.* 2006; Wittkopp *et al.* 2008) with a growing body of evidence for their direct role in speciation, particularly through transcription factors (Ting *et al.* 1998; Brideau *et al.* 2006; Mack and Nachman 2016). Here building on previous works which modelled the mechanistic basis and growth of DMIs in models of transcription factor DNA binding (Tulchinsky *et al.* 2014b,a; Khatri and Goldstein 2015a,b), we have investigated the growth of DMIs for a simple genotype-phenotype map of gene regulation for spatial patterning in embryonic development, previously studied in Khatri *et al.* (2009). Our results in this more complicated gene regulatory system confirm the basic conclusions from simple models of transcription factor binding (Khatri and Goldstein 2015a,b) that 1) as the population size decreases below the inverse of the characteristic scale of fitness ($2N\kappa_F \ll 1$) incompatibilities arise more quickly, 2) they grow in this regime as a quadratic power law with divergence time ($P_I \sim (\mu t)^2$) and 3) for large scaled population sizes incompatibilities arise more slowly with a characteristic negative curvature on a log-log plot indicative of a diffusive process. We note that although we find a quadratic growth of DMIs with divergence time (only at small scaled population sizes), which is as predicted by Orr's framework (Orr 1995), the underlying reason is very different in these models and arises as the common ancestor is likely to be close to the inviable region that gives non-functional binding (Khatri and Goldstein 2015b).

In the case of simple models of transcription factor DNA binding (Khatri and Goldstein 2015a,b), smaller diverging populations, or traits under weaker selection, were found to develop incompatibilities more quickly, as their common ancestor is already less well adapted due to sequence entropic pressures dominating fitness at smaller population sizes. Here we see that this basic principle that incompatibilities arise more quickly due to a higher drift load of the common ancestor remains valid for a more complicated gene regulatory system. Although this question requires greater empirical attention, there is direct and indirect evidence that smaller populations develop incompatibilities more quickly; for example, the greater species diversity in smaller habitats, such as Hawaii Mayr (1970), the island of Cuba Glor *et al.* (2004) and East African Great Lakes (Santos and Salzburger 2012; Owen *et al.* 1990), contrasted with the much slower speciation rate for animals with large ranges or population sizes (Mayr 1970, 1954; Rubinoff and Rubinoff 1971; Cooper and Penny 1997). In addition, there is more direct evidence from the net rates of diversification (Coyne and Orr 2004) inferred from phylogenetic trees (Nee 2001; Barraclough and Nee 2001), which support this population size trend.

The results of this model have also revealed a number of other emergent properties for the growth of hybrid incompatibilities, not obtainable by simply modelling transcription factor DNA binding. For example, for small populations we find clustering in the behaviours of growth of different types of DMIs, in particular, 3-point DMIs, which can be explained by the different sequence entropy constraints on different binding energies. Also we found that although the growth of DMIs at large population

bioRxiv preprint doi: https://doi.org/10.1101/123265; this version posted April 29, 2017. The copyright holder for this preprint (which was not certified by peer review) is the author/funder, who has granted bioRxiv a license to display the preprint in perpetuity. It is made available under aCC-BY 4.0 International license.

sizes has a characteristic negative curvature on a log-log plot, predicted theoretically by Khatri and Goldstein (2015a), indicating that hybrid traits randomly diffuse, a simple model of diffusion does not fit the simulation data well; instead a model of sub-diffusion, that would arise if there are a number of kinetic traps giving a broad distribution of substitution times, does fit the data well. This is consistent with the finding that the genotype-phenotype map has a rough fitness landscape, which is only revealed at sufficiently large population sizes (Khatri *et al.* 2009). These predictions can be tested empirically by more detailed studies of the divergence of species and their population size dependence, such as in Matute and Coyne (2010); Moyle and Nakazato (2010), which were used to test Orr's original prediction of quadratic growth of DMIs with divergence time.

However, most importantly we find that pair-wise or 2-point DMIs dominate compared higher order DMIs (3- and 4- point in this model with 4 loci). This is in contrast to Orr's theoretical argument that the fraction of viable paths from the common ancestor to the current day species increases as we consider higher order DMIs (Orr 1995). This argument partly rests on the assumption that the number of inviable genotypes remains fixed as a larger number of loci are considered, which would seem a very strong assumption. In the same paper Orr also argues that since there are $\binom{L}{n}$ possible $n-$point DMIs (the number of combinations of n loci amongst L loci), so as long as $n < L/2$, we would expect an increase in the number of DMIs as n increases; for $L = 4$ as in this paper, this would suggest 2-point DMIs are most numerous, potentially explaining the results we find. However, Orr's calculation in fact undercounts the number of DMIs, which as we showed above (see footnote) increases as $(2^n - 2)\binom{L}{n}$, in which case 3-point DMIs, would a priori be more numerous for 4 loci. Our results would then suggest, at least in this simple, but still relatively complex model, that biophysical constraints provide a stronger constraint on the relative number of DMIs of different orders than a purely combinatorial argument would suggest. Again evidence could be obtained from more detailed studies similar to Matute and Coyne (2010); Moyle and Nakazato (2010), where a power law with an exponent greater than 2 would indicate higher-order DMIs are dominant; currently this evidence suggests a quadratic growth law, however, a study with more time-points or species-pairs would provide more confidence. An alternative approach would be to look for linkage disequilibrium between unlinked regions hybrid genomes, such was found with hybrids of two species of swordtail fish Schumer *et al.* (2014), and though computationally challenging, compare this against evidence for and pervasiveness of higher order epistasis. Although recent results of Weinreich *et al.* (2013), would seem to contradict our conclusions, their finding of extensive complex epistasis relates to higher order interactions between sites within a single loci, coding for protein stability or enzymatic activity, whereas our work relates to epistasis between multiple loci.

There is an inherent simplicity with our gene regulatory module for spatial patterning, which requires only two proteins to bind to a regulatory region to turn on transcription; a key direction to investigate would be the effect of multiple transcription factors binding to enhancer regions to control gene expression (Bintu *et al.* 2005; Spitz and Furlong 2012; Levo and Segal 2014), where there could be a large scope for complex epistasis across many loci coding for a large number of transcription factors. However, as our results show, despite the possibility and a prior expectation of a larger number of triplet interactions, pair-wise interactions dominate; for complex transcriptional control, if pair-wise interactions between proteins, and proteins and DNA dominate, for example in determining the binding affinity of transcriptional complexes, then our conclusions would hold.

Overall, our results point to a basic principle, where developmental system drift or cryptic variation (True and Haag 2001; Haag 2014; Gavin-Smyth and Matute 2013), play a key role in speciation; basic body plans or phenotypes are conserved, but co-evolution of the components and loci of complicated gene regulatory networks can change differently in different lineages, giving incompatibilities that grow in allopatry. Here, we suggest a universal mechanism, where the rate of growth of incompatibilities is controlled by the drift load, or distribution of phenotypic values, of the common ancestor, which in turn is determined by a balance between selection pushing populations towards phenotypes of higher fitness and genetic drift pushing them towards phenotypes that are more numerous (higher sequence entropy). In particular, although in principle more complicated regulation could give rise to more complex patterns of epistasis (Orr 1995), our findings suggest that more simple, pair-wise, incompatibilities dominate the development of reproductive isolation between allopatric lineages under stabilising selection.

Supporting Information

Acknowledgments

We would like to thank Davis Pollock for initial discussions. RAG was supported by the Medical Research Council under grant U117573805 and BSK by The Francis Crick Institute which receives its core funding from Cancer Research UK, the UK Medical Research Council and the Wellcome Trust.

Literature Cited

Abzhanov, A., W. P. Kuo, C. Hartmann, B. R. Grant, P. R. Grant, and C. J. Tabin, 2006 The calmodulin pathway and evolution of elongated beak morphology in darwin's finches. Nature **442**: 563–567.

Barraclough, T. G. and S. Nee, 2001 Phylogenetics and speciation. Trends in Ecology & Evolution **16**: 391–399.

Bateson, W., 1909 pp. 85–101 in *Darwin and Modern Science*, edited by Seward, A., Cambridge University Press.

Bertin, E. and J.-P. Bouchaud, 2003 Subdiffusion and localization in the one-dimensional trap model. Physical Review E **67**: 026128.

Bintu, L., N. E. Buchler, H. G. Garcia, U. Gerland, T. Hwa, J. Kondev, and R. Phillips, 2005 Transcriptional regulation by the numbers: models. Curr Opin Genet Dev **15**: 116–124.

Brideau, N. J., H. A. Flores, J. Wang, S. Maheshwari, X. Wang, and D. A. Barbash, 2006 Two dobzhansky-muller genes interact to cause hybrid lethality in drosophila. science **314**: 1292–1295.

Brown, M., 1963 A generalized error function in n dimensions. Technical Report Technical Memorandum No. NMC-TM-63-8, U.S. Navy Missile Center.

Cooper, A. and D. Penny, 1997 Mass survival of birds across the cretaceous-tertiary boundary: molecular evidence. Science **275**: 1109–1113.

Coyne, J. A. and H. A. Orr, 2004 *Speciation*. Sinauer Associates, Inc.

Darwin, C. R., 1859 *The Origin of Species*. J. Murray, London.

bioRxiv preprint doi: https://doi.org/10.1101/123265; this version posted April 29, 2017. The copyright holder for this preprint (which was not certified by peer review) is the author/funder, who has granted bioRxiv a license to display the preprint in perpetuity. It is made available under aCC-BY 4.0 International license.

Dobzhansky, T., 1936 Studies on hybrid sterility. ii. localization of sterility factors in drosophila pseudoobscura hybrids. Genetics **21**: 113–135.

Eyre-Walker, A., M. Woolfit, and T. Phelps, 2006 The distribution of fitness effects of new deleterious amino acid mutations in humans. Genetics **173**: 891–900.

Fontana, W., 2002 Modelling 'evo-devo' with rna. Bioessays **24**: 1164–1177.

Gavin-Smyth, J. and D. R. Matute, 2013 Embryonic lethality leads to hybrid male inviability in hybrids between drosophila melanogaster and d. santomea. Ecology and evolution **3**: 1580–1589.

Glor, R. E., M. E. Gifford, A. Larson, J. B. Losos, L. R. Schettino, A. R. C. Lara, and T. R. Jackman, 2004 Partial island submergence and speciation in an adaptive radiation: a multilocus analysis of the cuban green anoles. Proceedings of the Royal Society of London B: Biological Sciences **271**: 2257–2265.

Goldstein, R. A., 2011 The evolution and evolutionary consequences of marginal thermostability in proteins. Proteins: Structure, Function, and Bioinformatics **79**: 1396–1407.

Greenbury, S. F., I. G. Johnston, A. A. Louis, and S. E. Ahnert, 2014 A tractable genotype–phenotype map modelling the self-assembly of protein quaternary structure. Journal of The Royal Society Interface **11**: 20140249.

Greenbury, S. F., S. Schaper, S. E. Ahnert, and A. A. Louis, 2016 Genetic correlations greatly increase mutational robustness and can both reduce and enhance evolvability. PLoS Comput Biol **12**: e1004773.

Haag, E. S., 2014 The same but different: worms reveal the pervasiveness of developmental system drift. PLoS Genet **10**: e1004150.

Hayden, E. J., E. Ferrada, and A. Wagner, 2011 Cryptic genetic variation promotes rapid evolutionary adaptation in an rna enzyme. Nature **474**: 92–95.

Higgs, P. G. and B. Derrida, 1992 Genetic distance and species formation in evolving populations. J Mol Evol **35**: 454–465.

Kauffman, S. and S. Levin, 1987 Towards a general theory of adaptive walks on rugged landscapes. J Theor Biol **128**: 11–45.

Khatri, B. S. and R. A. Goldstein, 2015a A coarse-grained biophysical model of sequence evolution and the population size dependence of the speciation rate. Journal of theoretical biology **378**: 56–64.

Khatri, B. S. and R. A. Goldstein, 2015b Simple biophysical model predicts faster accumulation of hybrid incompatibilities in small populations under stabilizing selection. Genetics **201**: 1525–1537.

Khatri, B. S., T. C. B. McLeish, and R. P. Sear, 2009 Statistical mechanics of convergent evolution in spatial patterning. Proc Natl Acad Sci U S A **106**: 9564–9569.

Kimura, M., 1962 On the probability of fixation of mutant genes in a population. Genetics **47**: 713–719.

King, M. C. and A. C. Wilson, 1975 Evolution at two levels in humans and chimpanzees. Science **188**: 107–116.

Lanfear, R., H. Kokko, and A. Eyre-Walker, 2014 Population size and the rate of evolution. Trends in ecology & evolution **29**: 33–41.

Levo, M. and E. Segal, 2014 In pursuit of design principles of regulatory sequences. Nature Reviews Genetics **15**: 453–468.

Mack, K. L. and M. W. Nachman, 2016 Gene regulation and speciation. Trends in Genetics .

MacKay, D. J. C., 2007 IV, p. 343 in *Information Theory, Inference, and Learning Algorithms*, Cambridge University Press.

Manrubia, S. and J. A. Cuesta, 2015 Evolution on neutral networks accelerates the ticking rate of the molecular clock. Journal of The Royal Society Interface **12**: 20141010.

Matute, D. R. and J. A. Coyne, 2010 Intrinsic reproductive isolation between two sister species of drosophila. Evolution **64**: 903–920.

Mayr, E., 1954 Geographic speciation in tropical echinoids. Evolution **8**: 1–18.

Mayr, E., 1970 18, pp. 347–350 in *Populations, Species, and Evolution*, Harvard University Press, Cambridge, Mass.

Moyle, L. C. and T. Nakazato, 2010 Hybrid incompatibility "snowballs" between solanum species. Science **329**: 1521–1523.

Muller, H., 1942 Isolating mechanisms, evolution and temperature. Biol. Symp. **6**: 71–125.

Nee, S., 2001 Inferring speciation rates from phylogenies. Evolution **55**: 661–668.

Ohta, T., 1973 Slightly deleterious mutant substitutions in evoluhypothesis by dna polymorphism. Genetics **123**: 585–595.

Ohta, T., 1992 The nearly neutral theory of molecular evolution. Annual Review of Ecology and Systematics **23**: 263–286.

Orr, H. A., 1995 The population genetics of speciation: the evolution of hybrid incompatibilities. Genetics **139**: 1805–1813.

Orr, H. A. and M. Turelli, 2001 The evolution of postzygotic isolation: accumulating dobzhansky-muller incompatibilities. Evolution **55**: 1085–1094.

Owen, R., R. Crossley, T. Johnson, D. Tweddle, I. Kornfield, S. Davison, D. Eccles, and D. Engstrom, 1990 Major low levels of lake malawi and their implications for speciation rates in cichlid fishes. Proceedings of the Royal Society of London B: Biological Sciences **240**: 519–553.

Rubinoff, R. W. and I. Rubinoff, 1971 Geographic and reproductive isolation in atlantic and pacific populations of panamanian bathygobius. Evolution pp. 88–97.

Santos, M. E. and W. Salzburger, 2012 Evolution. how cichlids diversify. Science **338**: 619–621.

Schaper, S. and A. A. Louis, 2014 The arrival of the frequent: how bias in genotype-phenotype maps can steer populations to local optima. PloS one **9**: e86635.

Schumer, M., R. Cui, D. L. Powell, R. Dresner, G. G. Rosenthal, and P. Andolfatto, 2014 High-resolution mapping reveals hundreds of genetic incompatibilities in hybridizing fish species. Elife **3**: e02535.

Shea, M. A. and G. K. Ackers, 1985 The or control system of bacteriophage lambda. a physical-chemical model for gene regulation. J Mol Biol **181**: 211–230.

Spitz, F. and E. E. Furlong, 2012 Transcription factors: from enhancer binding to developmental control. Nature Reviews Genetics **13**: 613–626.

Ting, C.-T., S.-C. Tsaur, M.-L. Wu, and C.-I. Wu, 1998 A rapidly evolving homeobox at the site of a hybrid sterility gene. Science **282**: 1501–1504.

True, J. R. and E. S. Haag, 2001 Developmental system drift and flexibility in evolutionary trajectories. Evolution & development **3**: 109–119.

Tulchinsky, A. Y., N. A. Johnson, and A. H. Porter, 2014a Hybrid incompatibility despite pleiotropic constraint in a sequence-based bioenergetic model of transcription factor binding. Genetics **198**: 1645–1654.

Tulchinsky, A. Y., N. A. Johnson, W. B. Watt, and A. H. Porter, 2014b Hybrid incompatibility arises in a sequence-based bioenergetic model of transcription factor binding. Genetics

bioRxiv preprint doi: https://doi.org/10.1101/123265; this version posted April 29, 2017. The copyright holder for this preprint (which was not certified by peer review) is the author/funder, who has granted bioRxiv a license to display the preprint in perpetuity. It is made available under aCC-BY 4.0 International license.

198: 1155–1166.

Weinreich, D. M., Y. Lan, C. S. Wylie, and R. B. Heckendorn, 2013 Should evolutionary geneticists worry about higher-order epistasis? Current opinion in genetics & development **23**: 700–707.

Wittkopp, P. J., B. K. Haerum, and A. G. Clark, 2008 Regulatory changes underlying expression differences within and between drosophila species. Nature genetics **40**: 346–350.

Wolf, J. B., J. Lindell, and N. Backström, 2010 Speciation genetics: current status and evolving approaches.

Wray, G. A., 2007 The evolutionary significance of cis-regulatory mutations. Nature Reviews Genetics **8**: 206–216.